Soft Matter

Accepted Manuscript

ROYAL SOCIETY OF CHEMISTRY

www.rsc.org/softmatter

Soft matter

RSCPublishing

ARTICLE

Nanoporous block copolymer films using highly selective solvents and non-solvent extraction

Cite this: DOI: 10.1039/xoxxoooooox

Changhuai Ye and Bryan D. Vogt

Received ooth January 2012,
Accepted ooth January 2012

DOI: 10.1039/xoxxoooooox

www.rsc.org/

Nanoporous block copolymer thin films are fabricated by selective solvent swelling of the majority phase and subsequent rapid extraction with a miscible non-solvent (water). Selection of the initial solvent provides a facile route to tune the porosity of the films. Poly(butylnorbornene)-block-poly(hydroxyhexafluoroisopropyl norbornene) (BuHFA) is used to generate these porous thin films due to its high T_g (>300 °C) and the selectivity of primary alcohols towards poly(hydroxyhexafluoroisopropyl norbornene) (pHFANB) to enable a relatively environmentally benign process. As the solvent quality for the HFA increases from ethanol to isopropanol to n-butanol, the porosity of the film developed by water extraction increases up to 69 %. Aqueous mixtures of ethanol provide an addition handle to tune the porosity between 10 and 54 %. These nanoporous films are robust with the porosity nearly unchanged after extended heating at 160 °C. Their elastic moduli are investigated using surface wrinkling and the modulus, E, scales with the film density, ρ, as $E \sim \rho^{2.2}$, which is similar to cellular solids. The nanopores are templated by the self-assembled structure of the block copolymer, so these coatings are transparent despite the high porosity. These thin films act as anti-reflective coatings for glass slides. Spin coating provides a coating on both sides and processing to generate 55 % porosity leads to an increase in transmittance from approximately 92% to 99.1% (average for the full range of visible light). A maximum transmittance of 99.8% is found at 523 nm. This methodology is simple and highly tunable; extension to other block copolymer systems is likely possible if sufficient solubility contrast between segments exists.

Introduction

The high pore density,[1] low dielectric constant[2] and low refractive index[3] of many nanoporous films make them attractive for a wide variety of applications including separation membranes,[4, 5] battery separators,[6] microelectronics[7] and anti-reflective coatings.[3, 8, 9] In general, the properties of nanoporous films critical to their efficacy in applications are the pore size, porosity, pore connectivity, and mechanical properties. The exact structure desired is driven by the application. For example, anti-reflective coatings require both high porosity (low refractive index) and small pore size (below diffraction limit).[8] One challenge to fabricate nanoporous polymeric films with high porosity (>50%) is their relatively weak mechanical properties that lead the collapse of the desired nanopore structure.[10, 11]

Block copolymers (BCPs) provide a facile route to nanoscale structures via self-assembly with the size tunable by the molecular weight.[12] Typically, the self-assembled system is post processed to selectively remove components to generate nanoporosity. Two common block copolymers that are compatible with direct chemical transformation are polystyrene-*block*-poly(methyl methacrylate) (PS-b-PMMA)[4] and polystyrene-*block*-polylactide (PS-b-PLA),[13] where PMMA can be degraded by UV exposure and PLA by hydrolytic degradation. Similarly, selective dissolution of homopolymers from block copolymer/homopolymer blends produces template nanopores.[6, 14]

Instead of processing to remove a component, solvent swelling can induce porous structure in block copolymers. Nanopores can be generated by selective swelling of block copolymers, such as PS-b-PMMA[15] or polystyrene-*block*-poly(2-vinyl pyridine) (PS-b-P2VP)[16, 17]. For example, the selective swelling of P2VP cylinders by ethanol leads to plastic deformation of majority PS phase to generate highly ordered nanopores after drying. Although this is a simple method, the porosity of these films is low (< 25%).[16] The porosity could be increased by swelling the majority phase and the minority phase used as the mechanical support during drying.

However, the challenge is preventing collapse of the swollen structure due to three factors. First, the mechanical properties of the solvent swollen BCP generally decreases significantly compared to the neat copolymer. Second, the magnitude of capillary force developed on evaporation increases as the pore size decreases, leading to a large applied stress.[18, 19] Third, as the porosity increase, the wall thickness decreases which further reduces resistance to deformation by external forces.[10] One alternative to increase the porosity is to combine self-assembly and non-solvent induced phase separation of triblock terpolymer system to produce hierarchically porous films.[20, 21] A similar hierarchically porous structure can be generated by spinodal decomposition of BCP blends that induces macro- and meso-phase separation.[22] Subsequent, selective dissolution yields a porous material. However, these hierarchically porous BCP films contain both macro- and nano-pores. For anti-reflective coatings, control of the pore size below the diffraction limit and high porosity are desired, but generally high porosity (>50 %) polymer films include pores that include large pores that diffract light and degrade performance in anti-reflective coatings.

In addition to its role in determining the stability of nanopores in soft materials, mechanical properties are critical for their ultimate use in applications. However, the mechanical properties are dependent on both the pore structure and porosity.[23, 24] For example, natural cellular solids exhibit a quadratic scaling relationship between modulus and density[23] while the modulus decreases more rapidly for highly porous organic aerogels with a 2.7 ± 0.2 scaling exponent between modulus and density.[25] The regularity in the material from ordered pore structures appear to improve the mechanical properties at high porosity. For example, the scaling exponents for cubic and hexagonal packed pores in nanoporous silica materials are 0.6 and 1.0, respectively.[26] These mechanical properties of nanoporous inorganic materials are generally studied by nanoindentation as the materials can be modeled as almost fully elastic.[27] However, nanoporous polymeric thin films are more difficult to assess with nanoindentation due to their low elastic modulus, viscoelasticity,[28] and substrate effects.[29] Stafford and coworkers developed a surface wrinkling technique that provides a facile way to measure the modulus of polymer thin films and porous inorganic films.[30] This surface wrinkling technique has been applied to a host of nanoscale materials with great success for elucidating their elastic moduli.[31]

Here, we seek to overcome some technical barriers associated with the generation of high porosity, nanoporous BCP films generated by selective solvent swelling using a novel BCP, poly(butylnorbornene)-block-poly(hydroxyhexafluoroisopropyl norbornene) (BuHFA). Both poly(butylnorbornene) (pBuNB) and poly(hydroxyl-hexafluoroisopropyl norbornene) (pHFANB) exhibit glass transition temperatures (T_g) greater than 300 ºC and also provide a significant solubility contrast for selective swelling. Moreover, this BCP appears to be highly conformationally asymmetric[32] as the symmetric block copolymer (on volume fraction basis) does not exhibit a lamellar morphology. This asymmetry enables the matrix of the BCP to be pHFANB, but maintaining a connected pBuNB framework during swelling that provides mechanical limitations to the swelling. Alcohols are highly selective for pHFANB and enable the generation of stable, high porosity (69%) BuHFA films by selective solvent swelling and subsequent solvent extraction by water. These porous polymer films are robust with a density-modulus scaling similar to natural cellular solids. These high porosity films provide anti-reflective properties for glass with >99 % transmission of visible light. These materials provide advantages in comparison to other porous polymer films in terms of high porosity, pore size control below diffraction limit, and high thermal stability of porous structure without crosslinking.

Experimental Section

Materials. 1-butanol (> 99%, ACS reagent), ethanol (> 99.5 %, ACS reagent), N, N-dimethylformamide (DMF, 99.8%), mesitylene (98%), and toluene (> 99.5 %, ACS reagent), were obtained from Sigma Aldrich and used as received. Isopropyl alcohol (> 99.0%, ACS reagent) was obtained from Macron Fine Chemicals and used as received.

For templating the porous films, two near-symmetric diblock copolymers of BuHFA were examined and obtained from Promerus LLC. ^{13}C NMR and GPC (Figure S1) were used to determine the molar compositions and the molecular weight. The densities of the respective homopolymers were measured using a helium pycnometer (Micromeritics Accupyc II 1340). The density of polyBuNB is 0.97 g/cm^3 while the density of polyHFANB is 1.42 g/cm^3, which is consistent with prior reports.[33] The characteristics of the BCPs are listed in Table 1. For nomenclature, the block copolymers are labeled as $BuHFA_f$, where *f* is the volume fraction of pHFANB in the copolymer.

Table 1 Block copolymer characteristics

	M_n (kg/mol)	PDI	BuNB:HFANB (mol:mol)	f_{HFA} (V/V)
$BuHFA_{0.50}$	106	1.18	0.55:0.45	0.50
$BuHFA_{0.59}$	74	2.09	0.46:0.54	0.59

Film preparation: The BuHFA copolymer along with 12 wt% (relative to polymer) of both DMF and mesitylene were dissolved in toluene to form a 3.5 wt% polymer solution. Silicon wafer pieces (1.5 cm × 1.5 cm, University Wafer, Inc) or glass slides (2.5 cm × 2 cm, VWR Microscope Slides) were used as substrates and cleaned using ultraviolet ozone (UVO, PSD Series Digital UV Ozone System, Novascan Technologies, Inc.) for 10 min before casting films. The BCP solutions were spun cast onto the cleaned substrates at 2500 rpm for 40 s. Subsequently, the films were annealed in a convection oven at 120 ℃ for 3 h to remove the residual solvent and improve the film adhesion with the substrate.

Pore fabrication: Scheme 1 pictorially illustrates the method by which the porous films are fabricated. The BuHFA thin film was immersed in the alcohol (or aqueous ethanoic solution) for 5 min. For the case of 1-butanol, the film was first immersed in butanol for 5 min, and then the films were quickly transferred to a beaker filled with ethanol for 3 min in order to exchange the butanol with ethanol. This additional step was needed due to the limited solubility of butanol in water. Subsequently

removing the films from the solvent, the films were quickly immersed in water for 2 min to extract the solvent rapidly. Finally, the films were dried with N_2 gas to obtain the porous thin films.

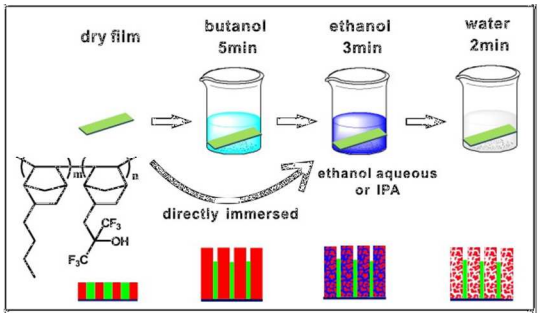

Scheme 1. Methods for fabrication of nanoporous BuHFA thin films

Film thickness and refractive index: A variable angle spectroscopic ellipsometer (VASE, J.A. Woollam Co., Inc) was used to measure the film thickness and refractive index of the supported films using a wavelength range from 300 nm to 1689 nm. The ellipsometric data were collected at 3 different angles (65°, 70° and 75°). The optical properties of the polymer films were obtained by fitting the ellipsometric data using a Cauchy model.

Morphology characterization: The surface morphology of the thin films was characterized by atomic force microscopy (AFM, diDimension V, Veeco) in tapping mode at a scan rate of 1 Hz. Scanning electron microscope (SEM, Model JEOL-7401) was used to characterize the porous structure of BuHFA thin films as both top-down images and cross-sections. Before imaging, the samples were coated with Ag for 2 min with a K575 sputter coater to prevent charging. Transmission electron microscopy (TEM) was also used to characterize the pore structure. The porous thin films were floated on water from silicon wafer and collected by TEM grids (300 mesh Cu, TED PELLA Inc). After drying in a vacuum oven at room temperature for 2 h, the films on TEM grids were characterized. To complement the microscopy characterization, grazing incidence small angle x-ray scattering (GISAXS) was used to characterize the as-cast and porous BuHFA thin films on the X9 beamline of National synchrotron Light Source (NSLS) at Brookhaven National Laboratory. An incident X-ray beam with energy of 13.5 keV and wavelength of 0.918 Å was used. Incident angles of 0.07 °, 0.10 °, 0.15 °, 0.2 ° and 0.3 ° were used for the GISAXS measurements.

Mechanical property measurement: The modulus of the porous BuHFA thin films was measured using surface wrinkling.[30] Poly(dimethyl siloxane) (PDMS, Sylgard 184, Dow Corning) with dimensions of 25 mm × 75 mm × 2 mm was used as the compliant substrate for wrinkling measurement. PDMS was prepared with ratio of base to curing agent of 20:1 (w:w) and cured at 120 °C for 3 h. The Young's modulus of the PDMS was measured using Texture Analyzer (TA-TX Plus) at a strain rate of 0.05 mm/s.

For surface wrinkling, the PDMS strips were pre-strained to 4.5 % and the porous BuHFA thin films were transferred from silicon wafer to PDMS. This transfer was assisted by immersion in water, while exploiting the differential adhesion of the film between the substrate and PDMS in water. After transfer, the polymer thin films were dried at ambient conditions for 12 h. Wrinkling was induced by releasing the pre-strain on PDMS at 0.1 mm/s using a Universal Motion Controller (Model: Esp100, Newport). The wrinkling was characterized using optical microscopy (Olympus MX51) and the wavelength was calculated using a fast Fourier transform (FFT) of the images. At least 8 micrographs were used to statistically calculate the wrinkle wavelength. At low strain, the modulus of the porous BuHFA film, $\bar{E}_f$, can be calculated from the wavelength, λ, as[34, 35]

$$\bar{E}_f = 3\bar{E}_s\left(\frac{\lambda}{2\pi h}\right)^3$$

where $\bar{E}_s$ is the plane-strain modulus of the PDMS substrate, and h is the film thickness.

UV-vis spectroscopy: The transmittance of blank and nanoporous BuHFA films coated glass slides was measured using a UV/Vis spectrophotometer (Model 8453, Hewlett-Packard/Agilent) over a wavelength range from 350 nm to 1000 nm.

Results and Discussion

Solvent swelling induced porous structure in block copolymer films. Figure 1A illustrates the morphology of the as-cast $BuHFA_{0.59}$ thin film. From the AFM micrographs, the as-cast film exhibits an unexpected morphology with many toroid-like structures arranged on an apparent hexagonal lattice, while the volume fraction of pHFANB is 0.59. At this composition, a lamellae or potentially gyroid morphology might be expected. To better assess the morphology, the GISAXS is used, which is consistent with perpendicular cylinders or hexagonally perforated lamellae. The limited ordering of the nanostructure inhibits unambiguous identification of the morphology. The lack of clear spill over behind the beamstop associated with a layered structure suggests perpendicular cylinder morphology.

pHFANB is soluble in lower alcohols, while pBuNB is only swollen by these alcohols. This significant difference in selectivity provides the basis for significant swelling for the fabrication of nanopores. When the $BuHFA_{0.59}$ thin film is immersed in butanol, the film does not dissolve, but is highly swollen. The butanol swelling appears to plastically deform the pBuNB phase as after butanol is exchanged with ethanol and then water (non-solvent for pHFANB), the porosity of the film is greater than porosity from swelling by ethanol alone. The

extraction of alcohol by water from the swollen $BuHFA_{0.59}$ film produces a porous structure and no further drying is necessary. Water in the last step of the fabrication of a highly porous material would generally destroy the porous structure by the large capillary stresses associated with the surface tension of water for most materials,[36] but as will be shown this processing can yield high porosity films for BuHFA. Ellipsometric measurements provide evidence for the creation of a porous structure by this processing as the thickness of the film expands from 187 nm to 510 nm and the refractive index decreases from 1.47 to 1.14. Intriguingly, additional drying at 120 °C for 2 h does not appreciably impact either the thickness or refractive index of the film. This result suggests that water extracts the ethanol out of the thin film without filling the pores. The porosity of the block copolymer thin films is determined from the change in refractive index by applying the Bruggemann effective medium approximation:[37, 38]

$$P\frac{n_1^2-n_{eff}^2}{n_1^2+2n_{eff}^2}+(1-P)\frac{n_2^2-n_{eff}^2}{n_2^2+2n_{eff}^2}=0$$

where n_1, n_2 and n_{eff} are the refractive indices of air, the skeletal block copolymer and porous block copolymer, respectively, and P is the volume fraction of voids in the nanoporous thin film. The porosity of porous $BuHFA_{0.59}$ thin film generated by swelling by butanol is 0.69. This is nearly three times the porosity reported previously for PS-b-P2VP generated by swelling by ethanol.[16]

Figure 1B shows the surface morphology of this porous $BuHFA_{0.59}$ film. The self-assembled morphology of the BCP is more evident in the porous film than the as-cast film. Moreover, examination of the height profile illustrates that the film goes from smooth for the as cast film to very rough associated with the formation of nanopores. More intriguingly, the GISAXS pattern indicates the structure of porous film changes substantially. The vertical streaks associated with perpendicular alignment are lost and a halo associated with a more isotropic structure appears. As pores are formed through a physical process, the porous structure in the block copolymer films can be removed by simply immersing the film in butanol drying directly in air (Figure 1C). Through this swelling/drying process, the refractive index of the $BuHFA_{0.59}$ film increases from 1.14 to 1.47, which is the same as as-cast $BuHFA_{0.59}$ film. However, the surface morphology of this non-porous $BuHFA_{0.59}$ film is similar to the porous $BuHFA_{0.59}$ film and some of the surface roughness remains, likely due to vitrification as the butanol evaporates. However, the internal structure appears to partially recover as determined by GISAXS (Figure 1C). Streaks associated with a perpendicularly aligned structure reappear, but the structure is not as well defined. Moreover, the d-spacing for recovered structure is only 80 nm, which is smaller than the as-cast film (93 nm) due to the loss of high boiling point solvents (DMF and mesitylene) from the as-cast film.

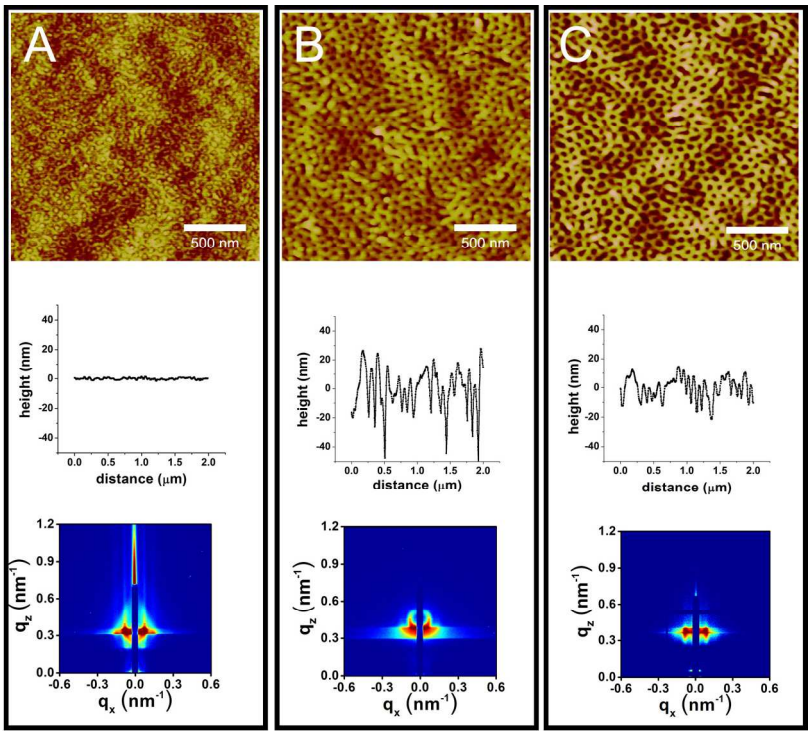

Figure 1. AFM height images, height profiles and GISAXS profiles of $BuHFA_{0.59}$ thin films with various processing. The (A) as-cast thin film is flat and exhibits an almost toroidal-like structure. Swelling with butanol, exchange with ethanol, and extraction with water yields a (B) porous thin film (P = 69%). If the porous film is immersed in butanol and dried, (C) a non-porous thin film is obtained illustrating the switchable nature of this swelling induced porosity.

Soft matter RSCPublishing

ARTICLE

The pores in the films are also characterized by electron microscopy as shown in Figure 2. Figure 2A illustrates the surface of the porous film via top-down SEM. The surface primarily contains circular pores, but there are some elongated pores, which are consistent with short parallel cylinders. Figure 2B illustrates the cross section of this film. The nanopores near the free surface are aligned perpendicularly to the plane of the film, while the pores within the film are more interconnected. The pore size is less than 50 nm as estimated from these micrographs. As water extraction appears to be the critical step to achieve a highly porous film, ethanol is also used to generate a nanoporous structure in $BuHFA_{0.59}$ films. In this case, the ethanol is directly extracted by water. The thickness $BuFHA_{0.59}$ film expands from 186 nm to 357 nm to produce 54 % porosity; this is significantly less porous than obtain when using butanol first to swell the film, but the porosity still is significantly greater than typically obtained from solvent induced swelling of block copolymers. This porosity is determined from the refractive index of the film. If one examines the apparent fraction of the film that is voids from the SEM micrographs, the volume of nanopores is significantly less (<< 50 %). This difference suggests that there is a significant fraction of microporosity (or at least pores <10 nm) based on the SEM micrographs. The surface morphology is very similar to that obtained from butanol (Figure S2B). Figure 2C illustrates the transmission image through the film thickness of this porous film. As this provides a projection of the structure through the full thickness of the film, the preferred perpendicular orientation at the surface is not clearly observed, by instead a relatively isotropic structure with a common size is present. The FFT of TEM micrograph confirmed this isotropic structure with a ring that defined the d-spacing of the structure (72 nm). The inset in Figure 2C illustrates the apparent interconnected nanostructure in more detail. This image represents a projection through 357 nm, so it is difficult to confirm the connectivity of the pores.

Tuning the porosity. In addition to the solvent used, the porosity of BuHFA thin films can also be tuned by changing the volume fraction of pHFANB in BuHFA thin films. As we are interested in high porosity films, two diblock copolymers with high pHFANB content, $BuHFA_{0.50}$ and $BuHFA_{0.59}$, are investigated using a series of alcohols for inducing porosity. Table 2 shows the characteristics of the porous films generated by swelling with alcohols and aqueous solvent extraction. The porosity of the film increases with increasing pHFANB content and increasing length of the alkyl chain of the alcohol. The highest porosity is obtained using butanol and the $BuHFA_{0.59}$. The porosity (69 %) calculated from the refractive index is similar to the thickness expansion (63 %). For ethanol, the porosity is still greater than 50 % for $BuHFA_{0.59}$, but lower porosities can be obtained by decreasing the solvent quality using aqueous ethanol solutions. By changing the ethanol content from 70 wt% to 100 wt%, the porosity can be tuned from 10% to 54%, which enables well defined refractive indices for these coatings.

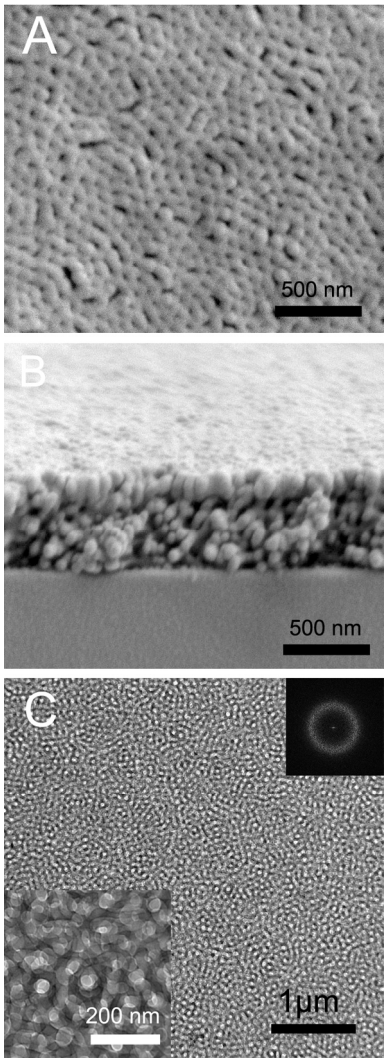

Figure 2. (A) Top-down and (B) cross-sectional SEM images of nanoporous $BuHFA_{0.59}$ thin film (P=69%) produced by swelling with butanol. (C) TEM micrographs through the porous $BuHFA_{0.59}$ film, P=0.54, produced by swelling with ethanol. Insets in (C) illustrate the higher magnification of TEM micrograph and the FFT of the micrograph. The porosity of the films are determined from the refractive index.

When decreasing the pHFANB content to 50 vol%, there is a marked decrease in the porosity of the films by nearly 40%

for both butanol and ethanol. Examination of the surface morphology by AFM indicates almost no difference in the structure (Figure S2) between $BuHFA_{0.50}$ and $BuHFA_{0.59}$. Thus, this difference appears to be predominately associated with the pHFANB content and the associated ability of the alcohol to swell the pHFANB domains and plasticize the pBuNB domains. To test this hypothesis, the $BuHFA_{0.50}$ was swollen by butanol at 80 °C, which increases its solubility in both phases of the BCP. With this processing, the porosity was increased substantially and greater than 50 % porosity can be obtained for this BCP as well.

Table 2. Processing and resulting porosity of block copolymer films

Block copolymer	Initial solvent[a]	Porosity (P)	n
	butanol	0.69	1.14
	IPA	0.57	1.19
	ethanol	0.54	1.21
BuHFA0.59	90 wt% ethanol	0.45	1.25
	80 wt% ethanol	0.35	1.30
	75 wt% ethanol	0.17	1.38
	70 wt% ethanol	0.10	1.42
	butanol (80 °C)	0.55	1.21
BuHFA0.50	butanol	0.44	1.27
	ethanol	0.32	1.33

[a] All solvents at 23 °C unless noted. All solutions are aqueous.

To better understand these differences in porosity, the swelling of the BCPs and pBuNB in butanol and ethanol are examined using spectroscopic ellipsometry. Figure 3 shows the solvent distribution in the films. For the homopolymer (pBuNB), the film swells 37 vol% in butanol and 22 vol% in ethanol. This swelling likely significantly reduces the modulus (1.1 GPa dry) and increases the ductility of the BuNB phase to enable the generation of such high porosity. Inclusion of the pHFANB increases the swelling significantly, but also leads to a heterogeneous solvent distribution in the film. Figure S3 illustrates the differences in the best fits of the ellipsometric angles for a uniform and heterogeneous solvent distribution. The accumulation of solvent near the substrate interface has been demonstrated previously for some homopolymers[39] and has been suggested as the source for thickness dependent swelling in BCP thin films.[40] The pHFANB phase likely preferentially wets the substrate due to the interactions with the surface silanols, which would provide additional swelling. There is nearly 53 vol % ethanol in $BuHFA_{0.50}$, which increases to 64 vol% ethanol for $BuHFA_{0.59}$. This nearly 11 % difference in swelling is less than the 22 % difference in porosity, which suggests there is some fixed loss in swelling by the process between the swollen state and the final porous state. This can be rationalized by the behavior of the films when the alcohol-swollen films are directly air dried. When directly drying the butanol-swollen BuHFA thin film in air, the thickness and refractive index of dried films are almost the same as the as-cast film, which suggests that no pores are formed. To explain these data, the forces associated with surface tension during evaporation of the butanol from the nanopores must be greater than the yield strength associated with the swollen pBuNB phase as pHFANB is soluble in alcohols. However, the rapid extraction of the alcohol by water results in removal of solvent from the pBuNB to provide sufficient strength to maintain the nanoporous structure.

Figure 3B illustrates the relationship between the extent of swelling and the porosity developed in these BCPs. The swelling fraction of the $BuHFA_{0.59}$ films decreases from 0.72 to 0.52 as the solvents used for swelling become more hydrophilic. However, the porosity decreases significantly from 0.69 to 0.17 as the swelling fraction decreases. This suggests the loss in swelling by the process between the swollen state and the final porous state also depends on the solvents swelling in the films.

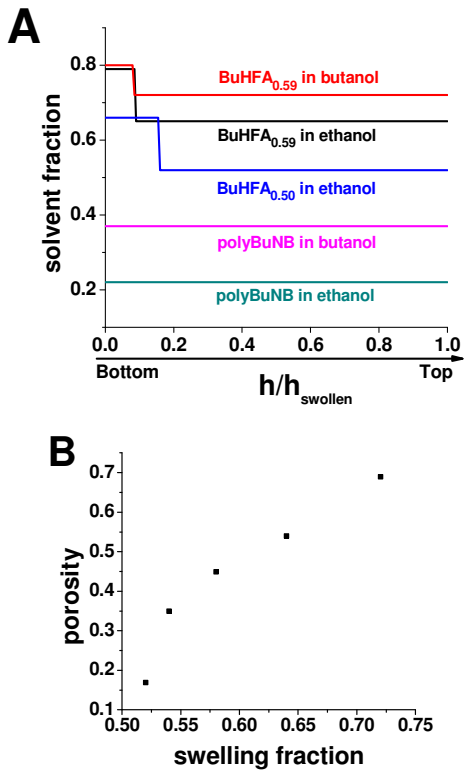

Figure 3. A) Solvent distribution in BCP films and polyBuNB homopolymer films determined from ellipsometry. B) Relationship between swelling and porosity of the $BuHFA_{0.59}$ copolymer films obtained by swelling using butanol or ethanol aqueous.

Mechanical properties of nanoporous films. The inclusion of porosity into any material decreases its mechanical properties. Surface wrinkling provides one facile route to study polymer thin films[41] as well as nanoporous silicate films.[34] Figure 4 illustrates the wrinkling of the nanoporous $BuHFA_{0.59}$ films that can be used to elucidate their elastic moduli from the wrinkle wavelength, λ. All films were initially approximately h = 180 nm thick, but after solvent exposure the thickness increases

proportionally to the porosity. However, it is clear that the wavelength of wrinkles does not significantly increase, while the film thickness increases significantly with increasing porosity. As the modulus scales as $(\lambda/h)^3$, the modulus of these nanoporous thin films must decrease dramatically as expected. However, the relationship between porosity and these properties, such as elastic modulus, depend dramatically on how the pores are arranged.[26] Changes in the extent of long range order of the nanopores can also substantially influence the modulus of inorganic films.[42] Quantification of the moduli enables this relationship to be assessed as shown in Figure 5.

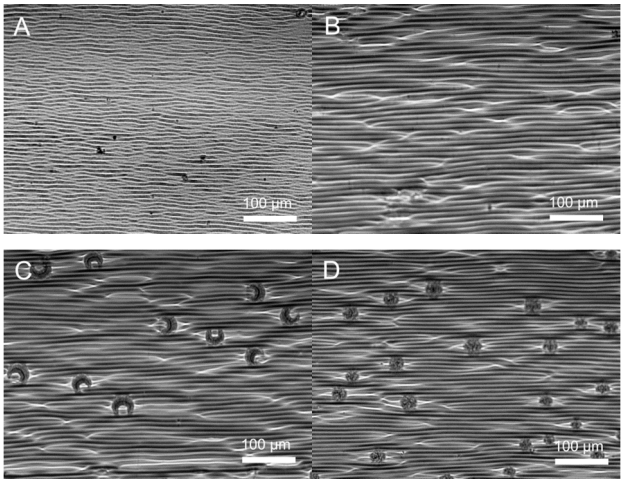

Figure 4. The wrinkling patterns of nanoporous $BuHFA_{0.59}$ thin films with varied porosities: (A) h = 510 nm, P = 69%, (B) h = 357 nm, P = 54%, (C) h = 245 nm, P=35%, (D) h =181 nm, P=10%.

The modulus of as-cast $BuHFA_{0.59}$ thin film is 1.45 GPa. The modulus of the nanoporous thin film with 69% porosity is only 41 MPa (3 % of non-porous film) and appears to be an outlier potentially due to the extreme distortion of the nanostructure required to obtain such a high porosity, or size dependent moduli[41] as the wall thickness must decrease as the porosity increases. It should be noted that we previously found no decrease in moduli for similar polynorbornenes for films as thin as 10 nm.[43] All other films follow a simple scaling with density as $E \sim \rho^{2.2}$. This scaling is similar to cellular solids ($E \sim \rho^{2.0}$) and worm-like disordered nanoporous silica ($E \sim \rho^{1.9}$),[26] which agrees with the morphology observed for the bulk of these films (Figure 2).

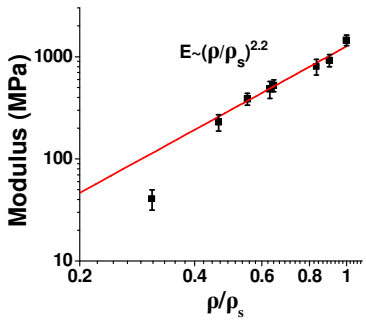

Figure 5. The relationship between the modulus and relative density of the nanoporous $BuHFA_{0.59}$ thin films. ρ and ρ_s are the density of porous $BuHFA_{0.59}$ and non-porous $BuHFA_{0.59}$. Both axes are on logarithmic scales.

Nanoporous BuHFA films as anti-reflective coatings. The transparent nature of these porous BCP films along with their highly tunable refractive indices (1.14 to 1.49) makes them attractive candidate for anti-reflective coatings to improve transmission. Maximizing the transmission requires (1) the light amplitudes reflected at both interfaces must be equal:

$$n_f = \sqrt{n_0 n_s}$$

where n_f, n_0 and n_s are refractive indices of anti-reflective coating, air and the substrate and (2) the reflected wave interfere destructively to incident wave:

$$d = \frac{\lambda}{4}$$

where d is the thickness of coating and λ is the wavelength of light. As the refractive index for glasses is approximately 1.5, the refractive index of anti-reflective coating should be approximately 1.22. Human eyes are most sensitive to 555 nm light, which provides the optimum thickness of the coating as 139 nm.

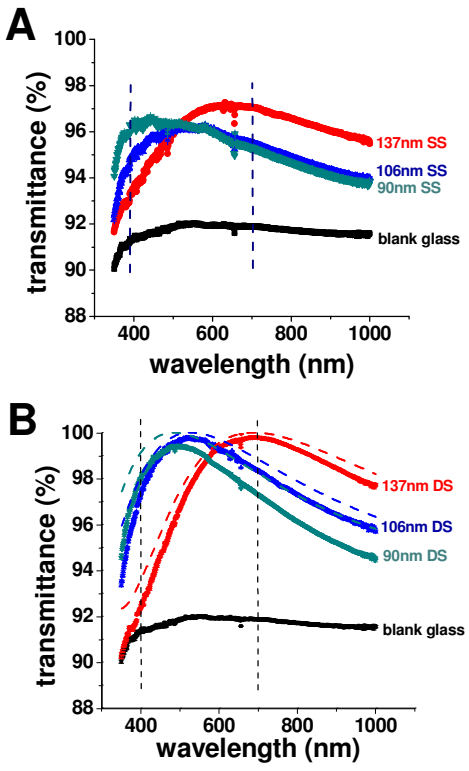

Figure 6. Transmittance of glass slides coated with (A) nanoporous $BuHFA_{0.50}$ thin film on single side (SS), (B) nanoporous $BuHFA_{0.50}$ thin films on both sides (DS). Vertical dashed lines denote the visible range. The dashed lines in B are calculated transmittances assuming the refractive index of the nanoporous films is 1.22 using characteristic matrix theory. In order to match the maxima in

transmittance, the thickness of the films were slightly varied from the ellipsometric measurement to 99, 110, and 141 nm.

The nanoporous thin films from butanol swollen $BuHFA_{0.50}$ thin film at 80 ℃ and ethanol swollen $BuHFA_{0.59}$ thin film match the required refractive index for maximizing transmission. Figure 6A illustrates the change in transmittance of a glass slide that is coated with nanoporous $BuHFA_{0.50}$ thin films. The refractive indices of these films with thicknesses of 90 nm, 106 nm and 137 nm are between 1.20 and 1.22 at λ = 633 nm. As shown in Figure 6, the transmittance of the glass substrate without coating is between 91 % - 92 % in the visible range (as denoted by vertical dashed lines). The transmittance increases in all cases to a maximum between 96% and 97% with the peak transmittance shifting to higher wavelengths for the thicker films as expected. The peaks are experimentally observed at higher wavelength than expected. As the surface of these coatings is rough as shown in Figure 2, ellipsometry might underestimate the thickness as reported previously for polymeric gratings.[44] Spin coating the substrates on both sides further reduces the light reflection. Figure 6B illustrates the transmittance of the double-side (DS) coated glass. In this case, the best performance is found for a 106 nm thick coating on both sides. The transmittance is greater than 97.3% across the visible range with an average of transmittance of 99.1% and the maximum transmittance, 99.8%, at 523 nm wavelength nearly matches the most sensitive wavelength (555 nm). This simple fabrication process provides a facile and effective way to produce anti-reflective coating.

The transmittance of the DS coated glass can be readily calculated from characteristic matrix theory as:[9,45]

$$R_L = \frac{(n_0 - n_s)^2 \cos^2\frac{\delta}{2} + (\frac{n_0 n_s}{n_f} - n_f)^2 \sin^2\frac{\delta}{2}}{(n_0 + n_s)^2 \cos^2\frac{\delta}{2} + (\frac{n_0 n_s}{n_f} + n_f)^2 \sin^2\frac{\delta}{2}}$$

where phase angle $\delta=(4\pi n_f d)/(\lambda\cos\theta)$. Here λ is the wavelength of incident light and θ is the incident angle of light. θ is 0° in the measurements in these cases. For the identical monolayers on both sides of the transparent substrate, the relationship between transmittance (T) and layer reflectance R_L can be described as:[46]

$$T = \frac{1 - R_L}{1 + R_L}$$

As shown in Figure 6B, this theory can generally describe the transmittance of the glass slide coated with the nanoporous films on each side. The effective thickness of the coating needs to be increased slightly. The theory overpredicts the transmittance and the difference between the measurement and theory increases as the film thickness decreases. This suggests that the porous film may not be uniform due to interfacial effects as the fraction of the film that is near the interface decreases as the film thickness increases.

The high glass transition temperature of the block copolymer components provides thermal stability for these anti-reflective coatings. Figure 7A illustrates the morphology of a nanoporous $BuHFA_{0.59}$ film (P = 60%) after heating at 160 ℃ for 12 h. The morphology is unchanged and the refractive index is almost unchanged decreasing slightly from 1.179 to 1.184, which corresponds to P = 59 % for the annealed film. This suggests the nanoporous polymer structure is exceptional for resisting high temperature deformation. This thermal stability provides excellent transmittance even after extended annealing at 160 ℃ as shown in Figure 7B. Note that the variance in the transmittance before and after heating is similar for a glass slide coated on both sides with a $BuHFA_{0.59}$ film if it is highly porous or is non-porous (no solvent treatment). The porous coating significantly outperforms the non-porous coating due to its lower refractive index.

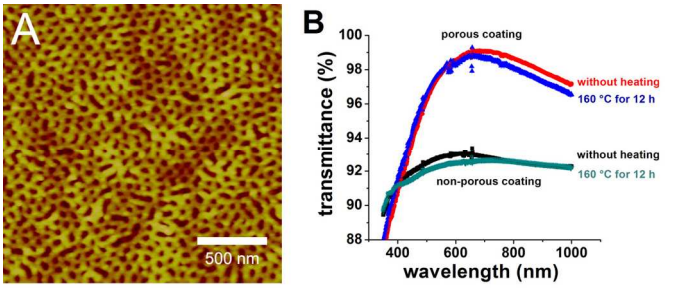

Figure 7. (A) AFM micrograph of nanoporous $BuHFA_{0.59}$ thin film (P= 0.59) after heating at 160 °C for 12 h. (B) Comparison of the transmittance before and after heating for a porous and non-porous $BuHFA_{0.59}$ thin film. The transmittance decreases to 98.7 % at 667 nm after heating.

Conclusions

Selective swelling of self-assembled BCP film followed by rapid water extraction was used to fabricate nanoporous polymeric films with tunable porosity. Unlike most aerogels, the water actually prevents porous structure collapse. The porosity of nanoporous $BuHFA_{0.59}$ block copolymer thin films can be tuned from 0% to 69% by simply changing the solvents. This porosity leads to decreased modulus that follows a scaling exponent of 2.2 with specific density, which is similar to that observed for cellular solids. The tunable porosity, moderate mechanical properties and high thermal resistance make these nanoporous BCP thin films attractive anti-reflective coatings. The transmittance increases from approximately 92% for uncoated glass to an average of 99.1% (visible range). These thermally robust porous films could find significant interest in a wide array of applications.

Acknowledgements

Research was carried out in part at the Center for Functional Nanomaterials, Brookhaven National Laboratory, which is supported by the U.S. Department of Energy, Office of Basic Energy Sciences, under Contract DE-AC02-98CH10886. The

authors thank A. Bell from Promerus, LLC for providing the norbornene-based block copolymers and thank Zhe Qiang, Sarang Bhaway, Yuanzhong Zhang and Kevin Yager for their assistance with the GISAXS measurements. The authors express their gratitude to Yan Sun and Yuwei Chen for assistance with UV-vis spectroscopy and SEM measurements.

Notes and references

[a] Department of Polymer Engineering, University of Akron, Akron, OH 44325

† Electronic Supplementary Information (ESI) available: GPC and ^{13}C NMR spectrum of $BuHFA_{0.50}$ and $BuHFA_{0.50}$, AFM images of as-cast $BuHFA_{0.50}$ and $BuHFA_{0.50}$ films and corresponding porous films obtained from swelling by ethanol and butanol, and the differences in the best fits of the ellipsometric angles for a uniform and heterogeneous solvent distribution for $BuHFA_{0.59}$ thin film swollen by ethanol. See DOI: 10.1039/b000000x/

1. R. M. Dorin, W. A. Phillip, H. Sai, J. Werner, M. Elimelech and U. Wiesner, *Polymer*, 2014, **55**, 347-353.
2. J. L. Hedrick, R. D. Miller, C. J. Hawker, K. R. Carter, W. Volksen, D. Y. Yoon and M. Trollsas, *Adv. Mater.*, 1998, **10**, 1049-1053.
3. G. Wicht, R. Ferrini, S. Schuttel and L. Zuppiroli, *Macromol. Mater. Eng.*, 2010, **295**, 628-636.
4. S. Y. Yang, J. Park, J. Yoon, M. Ree, S. K. Jang and J. K. Kim, *Adv. Funct. Mater.*, 2008, **18**, 1371-1377.
5. Z. G. Wang, X. P. Yao and Y. Wang, *J. Mater. Chem.*, 2012, **22**, 20542-20548.
6. D. T. Wong, C. Wang, J. A. Pople and N. P. Balsara, *Macromolecules*, 2013, **46**, 4411-4417.
7. G. D. Fu, B. Y. Zong, E. T. Kang and K. G. Neoh, *Ind. Eng. Chem. Res.*, 2004, **43**, 6723-6730.
8. S. Walheim, E. Schaffer, J. Mlynek and U. Steiner, *Science*, 1999, **283**, 520-522.
9. W. Joo, M. S. Park and J. K. Kim, *Langmuir*, 2006, **22**, 7960-7963.
10. C. H. Ye, Y. W. Luo and X. S. Liu, *Polymer*, 2011, **52**, 683-693.
11. X. A. Li, L. J. Xue and Y. C. Han, *J. Mater. Chem.*, 2011, **21**, 5817-5826.
12. S. B. Darling, *Prog. Polym. Sci.*, 2007, **32**, 1152-1204.
13. B. Gorzolnik, P. Davidson, I. Beurroies, R. Denoyel and D. Grande, *Macromol. Symp.*, 2010, **287**, 127-134.
14. U. Y. Jeong, H. C. Kim, R. L. Rodriguez, I. Y. Tsai, C. M. Stafford, J. K. Kim, C. J. Hawker and T. P. Russell, *Adv. Mater.*, 2002, **14**, 274-276.
15. T. Xu, J. Stevens, J. A. Villa, J. T. Goldbach, K. W. Guarim, C. T. Black, C. J. Hawker and T. R. Russell, *Adv. Funct. Mater.*, 2003, **13**, 698-702.
16. J. Yin, X. P. Yao, J. Y. Liou, W. Sun, Y. S. Sun and Y. Wang, *ACS Nano*, 2013, **7**, 9961-9974.
17. Y. Wang, L. Tong and M. Steinhart, *ACS Nano*, 2011, **5**, 1928-1938.
18. V. Muralidharan and C. Y. Hui, *Macromol. Rapid Comm.*, 2004, **25**, 1487-1490.
19. M. Visscher, J. Laven and R. van der Linde, *Prog. Org. Coat.*, 1997, **31**, 311-323.
20. W. A. Phillip, R. M. Dorin, J. Werner, E. M. V. Hoek, U. Wiesner and M. Elimelech, *Nano Lett.*, 2011, **11**, 2892-2900.
21. K. V. Peinemann, V. Abetz and P. F. W. Simon, *Nat. Mater.*, 2007, **6**, 992-996.
22. H. Sai, K. W. Tan, K. Hur, E. Asenath-Smith, R. Hovden, Y. Jiang, M. Riccio, D. A. Muller, V. Elser, L. A. Estroff, S. M. Gruner and U. Wiesner, *Science*, 2013, **341**, 530-534.
23. L. J. Gibson, *J. Biomech.*, 1985, **18**, 317-328.
24. G. Lu, G. Q. M. Lu and Z. M. Xiao, *J. Porous Mat.* 1999, **6**, 359-368.
25. R. W. Pekala, C. T. Alviso and J. D. Lemay, *J. Non-Cryst. Solids*, 1990, **125**, 67-75.
26. H. Fan, C. Hartshorn, T. Buchheit, D. Tallant, R. Assink, R. Simpson, D. J. Kisse, D. J. Lacks, S. Torquato and C. J. Brinker, *Nat. Mater.*, 2007, **6**, 418-423.
27. B. Y. Du, O. K. C. Tsui, Q. L. Zhang and T. B. He, *Langmuir*, 2001, **17**, 3286-3291.
28. M. R. VanLandingham, J. S. Villarrubia, W. F. Guthrie and G. F. Meyers, *Macromol. Symp.*, 2001, **167**, 15-43.
29. S. Watcharotone, C. D. Wood, R. Friedrich, X. Chen, R. Qiao, K. Putz and L. C. Brinson, *Adv. Eng. Mater.*, 2011, **13**, 400-404.
30. J. Y. Chung, A. J. Nolte and C. M. Stafford, *Adv. Mater.*, 2011, **23**, 349-368.
31. J. A. Howarter and C. M. Stafford, *Soft Matter*, 2010, **6**, 5661-5666.
32. F. S. Bates, M. F. Schulz, A. K. Khandpur, S. Forster, J. H. Rosedale, K. Almdal and K. Mortensen, *Faraday Discuss.*, 1994, **98**, 7-18.
33. K. D. Dorkenoo, P. H. Pfromm and M. E. Rezac, *J. Polym. Sci. B-Polym. Phys.*, 1998, **36**, 797-803.
34. C. M. Stafford, C. Harrison, K. L. Beers, A. Karim, E. J. Amis, M. R. Vanlandingham, H. C. Kim, W. Volksen, R. D. Miller and E. E. Simonyi, *Nat. Mater.*, 2004, **3**, 545-550.
35. C. M. Stafford, S. Guo, C. Harrison and M. Y. M. Chiang, *Rev. Sci. Instru.*, 2005, **76**, 062207.
36. S. Bandi, M. Bell and D. A. Schiraldi, *Macromolecules*, 2005, **38**, 9216-9220.
37. D. E. Aspnes, *Thin Solid Films*, 1982, **89**, 249-262.
38. H. Y. Hsueh, H. Y. Chen, M. S. She, C. K. Chen, R. M. Ho, S. Gwo, H. Hasegawa and E. L. Thomas, *Nano Lett.*, 2010, **10**, 4994-5000.
39. B. D. Vogt, V. M. Prabhu, C. L. Soles, S. K. Satija, E. K. Lin and W. L. Wu, *Langmuir*, 2005, **21**, 2460-2464.
40. U. Zettl, A. Knoll and L. Tsarkova, *Langmuir*, 2010, **26**, 6610-6617.
41. C. M. Stafford, B. D. Vogt, C. Harrison, D. Julthongpiput and R. Huang, *Macromolecules*, 2006, **39**, 5095-5099.
42. X. Li, L. Song and B. D. Vogt, *J. Phys. Chem. C*, 2008, **112**, 53-60.
43. J. M. Torres, C. Wang, E. B. Coughlin, J. P. Bishop, R. A. Register, R. A. Riggleman, C. M. Stafford and B. D. Vogt, *Macromolecules*, 2011, **44**, 9040-9045.
44. J. H. Lee, H. W. Ro, R. Huang, P. Lemaillet, T. A. Germer, C. L. Soles and C. M. Stafford, *Nano Lett.*, 2012, **12**, 5995-5999.
45. M. J. Minot, *J. Opt. Soc. Am.*, 1976, **66**, 515-519.
46. E. Hild, A. Deak, L. Naszalyi, O. Sepsi, N. Abraham, Z. Horoelgyi, *J. Opt. A- Pure Appl. Op.*, 2007, **9**, 920-930.

Table of content

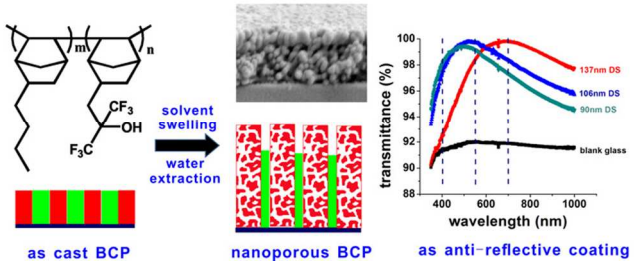

Selective swelling of matrix by alcohol followed by rapid extraction by the non-solvent water leads to a highly porous film with tunable optical properties. These films exhibit anti-reflective properties and are thermally robust.